THE FASEB JOURNAL • RESEARCH • www.fasebj.org

Role of intracellular Ca^{2+}–based mechanotransduction of human periodontal ligament fibroblasts

Ei Ei Hsu Hlaing,* Yoshihito Ishihara,†,1 Ziyi Wang,*,‡ Naoya Odagaki,† and Hiroshi Kamioka*

*Department of Orthodontics, Okayama University Graduate School of Medicine, Dentistry, and Pharmaceutical Sciences, Okayama, Japan; †Department of Orthodontics, Okayama University Hospital, Okayama, Japan; and ‡Japan Society for the Promotion of Science (JSPS DC2), Tokyo, Japan

ABSTRACT: Human periodontal ligament (hPDL) fibroblasts are thought to receive mechanical stress (MS) produced by orthodontic tooth movement, thereby regulating alveolar bone remodeling. However, the role of intracellular calcium ($[Ca^{2+}]_i$)-based mechanotransduction is not fully understood. We explored the MS-induced $[Ca^{2+}]_i$ responses both in isolated hPDL fibroblasts and in intact hPDL tissue and investigated its possible role in alveolar bone remodeling. hPDL fibroblasts were obtained from healthy donors' premolars that had been extracted for orthodontic reasons. The oscillatory $[Ca^{2+}]_i$ activity induced by static compressive force was measured by a live-cell Ca^{2+} imaging system and evaluated by several feature extraction method. The spatial pattern of cell-cell communication was investigated by Moran's *I*, an index of spatial autocorrelation and the gap junction (GJ) inhibitor. The Ca^{2+}-transporting ionophore A23187 was used to further investigate the role of $[Ca^{2+}]_i$ up-regulation in hPDL cell behavior. hPDL fibroblasts displayed autonomous $[Ca^{2+}]_i$ responses. Compressive MS activated this autonomous responsive behavior with an increased percentage of responsive cells both *in vitro* and *ex vivo*. The integration, variance, maximum amplitude, waveform length, and index *J* in the $[Ca^{2+}]_i$ responses were also significantly increased, whereas the mean power frequency was attenuated in response to MS. The increased Moran's *I* after MS indicated that MS might affect the pattern of cell-cell communication *via* GJs. Similar to the findings of MS-mediated regulation, the A23187-mediated $[Ca^{2+}]_i$ uptake resulted in the up-regulation of receptor activator of NF-κB ligand (Rankl) and Sost along with increased sclerostin immunoreactivity, suggesting that $[Ca^{2+}]_i$ signaling networks may be involved in bone remodeling. In addition, A23187-treated hPDL fibroblasts also showed the suppression of osteogenic differentiation and mineralization. Our findings suggest that augmented MS-mediated $[Ca^{2+}]_i$ oscillations in hPDL fibroblasts enhance the production and release of bone regulatory signals *via* Rankl/Osteoprotegerin and the canonical Wnt/β-catenin pathway as an early process in tooth movement–initiated alveolar bone remodeling.—Ei Hsu Hlaing, E., Ishihara, Y., Wang, Z., Odagaki, N., Kamioka, H. Role of intracellular Ca^{2+}–based mechanotransduction of human periodontal ligament fibroblasts. FASEB J. 33, 10409–10424 (2019). www.fasebj.org

KEY WORDS: hPDL · intracellular calcium · SOST/sclerostin · Rankl/Opg · bone remodeling

Cells and tissues sense physical, chemical, and biologic stimuli and adapt to their local environment. Cellular mechanotransduction, the process by which the cells convert mechanical signals into biochemical signals and gene expression, is critical for modulating normal homeostasis in physiologic functions of living organisms (1). Periodontal ligament (PDL) fibroblasts are highly dominant cellular components in human PDL (hPDL) tissue, which surrounds the tooth roots and connects to the alveolar bone (2). These fibroblasts continuously adapt to mechanical stress (MS) generated by mastication, speech, or orthodontic tooth movement (OTM), which leads to remodeling of both the ligament and its surrounding alveolar bone (3, 4). Such remodeling activity has been suggested to be initiated by mechanotransduction pathways and then be transformed into intracellular biochemical signals, such as prostaglandins,

ABBREVIATIONS: 18α-GA, 18 α-glycyrrhetinic acid; $[Ca^{2+}]_i$, intracellular calcium; GAPDH, glyceraldehyde-3-phosphate dehydrogenase; GJ, gap junction; HE, hematoxylin and eosin; HIFBS, heat-inactivated fetal bovine serum; hPDL, human PDL; Int, integration; MA, maximum amplitude; MPF, mean power frequency; MS, mechanical stress; Opg, osteoprotegerin; Osx, osterix; OTM, orthodontic tooth movement; PCA, principal components analysis; PDL, periodontal ligament; qRT-PCR, quantitative RT-PCR; Rankl, receptor activator of NF-κB ligand; rJ, the ratio of the activity during the treatment and under control conditions; Runx2, runt-related transcription factor 2; Var, variance; WL, waveform length

[1] Correspondence: Department of Orthodontics, Okayama University Hospital, 2-5-1 Shikata-cho, Kita-ku, Okayama City, Okayama 700-8558, Japan. E-mail: ishihara@md.okayama-u.ac.jp

doi: 10.1096/fj.201900484R
This article includes supplemental data. Please visit *http://www.fasebj.org* to obtain this information.

neurotransmitters, cytokines, and intracellular calcium ($[Ca^{2+}]_i$) mobilization (5–8).

Several previous studies have reported the transduction of mechanical signals into biologic responses of hPDL fibroblasts. When the mechanical force is applied, hPDL fibroblasts on the compressed side release osteoclast inductive molecules, such as receptor activator of NF-κB ligand (Rankl) or IL-1, to maintain the optimal PDL distance (9–11). Our previous study also showed that compressive MS increases PDL-derived sclerostin, a negative regulator of bone formation through antagonizing Wnt/β-catenin signaling, and biphasically regulates the expression of Sost (encoding sclerostin) in a force-dependent manner in isolated hPDL cells (12).

Ca^{2+} is an important second messenger of signal transduction (13), and $[Ca^{2+}]_i$ mobilization is one of the earliest events in the cellular mechanotransduction process of translating mechanical stimuli to biochemical signals, thereby activating various physiologic cellular functions (14). Previous studies have shown the transient elevation of $[Ca^{2+}]_i$ concentration in response to MS from isolated gingival or PDL fibroblasts *in vitro* (15, 16). However, this form of spatiotemporal organization of signaling has been demonstrated neither in hPDL fibroblasts nor in intact hPDL tissue. Furthermore, a concise overview of MS-mediated biologic regulation *via* $[Ca^{2+}]_i$ signaling networks of hPDL fibroblasts has yet to be established.

In OTM, the application of MS onto the tooth is transduced to the PDL, then PDL fibroblasts release the biologic mediators, which trigger the remodeling of the adjacent alveolar bone by signaling the surrounding cells (17). We therefore hypothesized that $[Ca^{2+}]_i$ in hPDL fibroblasts is modulated by compressive MS, thereby regulating the tooth movement–initiated alveolar bone remodeling process. To validate this hypothesis, we investigated compressive force–induced $[Ca^{2+}]_i$ transients in both hPDL explants and primary isolated fibroblasts. In addition, we examined the molecular mechanisms by which the activation of $[Ca^{2+}]_i$ transients affect the gene expression profiles as well as osteogenic differentiation.

MATERIALS AND METHODS

Culture of *ex vivo* hPDL explants

hPDLs were collected from healthy donors' premolars that had been extracted for orthodontic reasons at Okayama University Hospital, as previously described (12). The hPDLs were dissected into 2-mm pieces for further use. The explants were subsequently incubated in α–minimal essential medium (Thermo Fisher Scientific, Waltham, MA, USA) supplemented with 10% heat-inactivated fetal bovine serum (HIFBS; HyClone Laboratories, Logan, UT, USA), 100 U/ml penicillin, and 100 μg/ml streptomycin (Thermo Fisher Scientific) at 37°C. The protocol for this experiment was approved by the Institutional Ethics Committee of Okayama University (KEN1701-024).

hPDL cell isolation, culture, and osteogenic differentiation

The hPDL fibroblasts were isolated from extracted premolars as previously described by Kawanabe *et al.* (18). The cells were plated on double-coated glass bottom dishes (Matsunami, Osaka, Japan) for microscopic observation or plastic cell culture dishes (Greiner, Kremsmünster, Austria) and then cultured in 10% HIFBS with antibiotics. Cultures were also treated with A23187 (MilliporeSigma, Burlington, MA, USA), a Ca^{2+}-transporting ionophore, or vehicle (PBS) to evaluate the role of $[Ca^{2+}]_i$ signal in primary cultured hPDL fibroblasts at the indicated concentrations. 18 α-glycyrrhetinic acid (18α-GA; MilliporeSigma), a gap junction (GJ) inhibitor, was used to examine the involvement of GJ-mediated intercellular communication on the MS-induced $[Ca^{2+}]_i$ dynamics as previously described (19, 20). To visualize mineralized nodule formation, cells were replated in 12-well plates, and differentiation was initiated 24 h after plating by replacing the growth medium with 10% HIFBS and antibiotics, including 0.05 mM L-ascorbic acid, 100 nM dexamethasone, and 10 mM β-glycerophosphate (all obtained from MilliporeSigma). After 14 d of culture, cells were fixed with 70% ethanol at −20°C and stained with 40 mM alizarin red stain solution (pH = 4.2; MilliporeSigma). Passages 2–6 of primary isolated hPDL fibroblasts were used in this experiment.

Dye loading and live-cell imaging

The oscillatory $[Ca^{2+}]_i$ activity was measured in Fluo8-AM–loaded (10 μM for 15 min at 37°C) hPDL explants or isolated hPDL fibroblasts, as previously described (21). Fluorescence images of cells were acquired with a FluoView FV500 confocal laser scanning microscopy system (Olympus, Tokyo, Japan). The scanning rate was 1.12 s/scan for 8-bit images 512 × 512 pixels in size. Time-lapse images collected from a single Z plane were recorded at 3-s intervals. The fluorescence activity in the cells before the application of MS was regarded as 1.

Application of static compressive force

MS was applied to the hPDL explants or isolated hPDL fibroblasts by the uniform compression method, as previously described (12). Different magnitudes of glass cylinders (0.24, 2.40 g/cm^2) were placed over a confluent cell layer in the medium, which were determined in the same manner as previously described (12, 22) for the physiologic range of MS in bone remodeling.

Processing and analyses of $[Ca^{2+}]_i$ signals

The subtract background method embedded in the ImageJ/Fiji tool (*https://fiji.sc/*) was used to neutralize the background of live-cell time-lapse images (23). All cells on the images were then outlined with the polygon selections region-of-interest tool to avoid bias. Finally, the $[Ca^{2+}]_i$ signals of all cells were extracted using a macro script (*https://github.com/wong-ziyi/imagej_wzy_timeLapse*) in ImageJ/Fiji that was developed by the authors.

The $[Ca^{2+}]_i$ signals feature was extracted using several methods widely applied for surface electromyography signal processing and classification: integration (Int), variance (Var), waveform length (WL), maximum amplitude (MA), and mean power frequency (MPF) (24, 25). The mathematical representation of these methods is:

$$\text{Int} = \sum_{n=1}^{N} |X_n| \quad (1)$$

$$\text{Var} = \frac{1}{N-1} \sum_{n=1}^{N} {x_n}^2 \quad (2)$$

$$\text{WL} = \sum_{n=1}^{N} |x_{n+1} - x_n| \quad (3)$$

$$\text{MA} = \max_{1 \le n \le N} x_n - \min_{1 \le n \le N} x_n \quad (4)$$

$$\text{MPF} = \sum_{n=1}^{N} f_n P_n / \sum_{n=1}^{N} P_n \quad (5)$$

where N is the length of the $[Ca^{2+}]_i$ signals, x_n represents the $[Ca^{2+}]_i$ signal from image n of the time-lapse images, and f_n and P_n are the frequency value and power spectrum, respectively, of the $[Ca^{2+}]_i$ signal power spectrum at the frequency segment n. Before the feature extraction, all original $[Ca^{2+}]_i$ signals were mean-centered.

In addition, the recently developed index J method (26) was also applied to quantitatively evaluate the $[Ca^{2+}]_i$ activity. In brief, the original trace $f(t)$ was taken to be mean-centered (see Fig. 3*A*, middle panel, upper box), and then its wavelet transform $W(a,b) = |a|^{-1/2} \int \psi^*[(t-b)/a] f(t) \mathrm{d}t$ was computed according to Eq. 2 of Ruffinatti *et al.* (26) as a function of time b and scale a (*denotes complex conjugation). The Morlet function $\psi(t) \approx \pi^{-1/4} \exp(-0.5t^2) \exp(ist)$ was used as the mother wavelet [s is a constant parameter; $s = 5$ in our case; see Eqs. 3–5 of Ruffinatti *et al.* (26)]. To obtain a representation of the signal in the time-frequency domain, b was renamed t and substitution was performed for $v = s/(2\pi a)$. The resulting scaleogram $|W(t,v)|$ was plotted with an appropriate pseudocolor table (see Fig. 3*A*, middle panel, middle box). The index $J(t) \approx \int |W(t,v)|^2 v \mathrm{d}v$ was then calculated as formally defined in Eq. 9 of Ruffinatti *et al.* (26) and plotted as a function of time (see Fig. 3*A*, middle panel, lower box), thereby providing a reliable estimate of the oscillatory activity of the signal $f(t)$. Finally, for each temporal window of interest (*i.e.*, control, A23187, 18α-GA, and compression), the mean J ($\langle J \rangle$) was calculated in order to estimate the $[Ca^{2+}]_i$ activity as the ratio of the activity during the treatments (A23187, 18α-GA, or compression) and under control conditions (ctrl): $r_J = \langle J \rangle_{treatment} / \langle J \rangle_{ctrl}$ [as defined in Eqs. 10 and 11 of Ruffinatti *et al.* (26)]. In this way, we defined responding cells as $r_J > 1$ and nonresponding ones as $r_J \le 1$.

To investigate the synchronization of the $[Ca^{2+}]_i$ activity among cells, Moran's I was used to estimate the spatial autocorrelation of each previous signal feature (Int, Var, WL, MA, MPF, and index J) (27). Spatial autocorrelation generally describes the correlation of the values of a certain variable among spatial units (PDL cells in our case). If neighboring units tend to have similar values, these spatial units are positively related, whereas they are negatively related if they tend to have dissimilar values. As in the examples shown in Fig. 3*A* (right panel), a Moran's I closer to ±1 more strongly indicates the existence of spatial dependence, whereas no dependence is suggested if Moran's I is closer to 0. Moran's I is defined by the following formula:

$$\text{Moran's } I = \frac{1}{\sum_{ij} w_{ij}} \frac{\sum_{ij} w_{ij} (X_i - \bar{X})(X_j - \bar{X})}{N^{-1} \sum_i (X_i - \bar{X})^2}$$

where N denotes the number of observables or spatial units (PDL cells in our case); $X_i, i = 1, 2, \ldots, N$, $\bar{X} = \frac{1}{N} \sum_i X_i$ is the mean of X_i; and w_{ij} is a matrix of inverse distance weights between the i-th and j-th observables in which each off-diagonal entry $[i, j]$ in the matrix is equal to 1/(distance between point i and point j) and the diagonal entry with a value of 0.

To focus on the initial stage of the response to MS, all of the above measurements were based only on the $[Ca^{2+}]_i$ profile obtained within 2 min in both the control and treatment groups. All of the above measurements were calculated by a specialized software program (*https://github.com/wong-ziyi/R_Wave_analysis*) that was developed by Dr. Ziyi Wang using the shiny package for *R* and several open source packages (*e.g.*, ape, biwavelet, and pracma) of *R*. A ward clustering heatmap and principal components analysis (PCA) were applied to show the different patterns of $[Ca^{2+}]_i$ activity based on the 6 wave features using a singular value decomposition algorithm.

Evaluation of cell viability

The dual dye uptake assay for the estimation of cell viability was previously described (19). In brief, isolated hPDL fibroblasts were loaded with 5.0 μM Calcein-AM (Molecular Probes, Eugene, OR, USA) and 5 mg/ml propidium iodide (Molecular Probes) for 15 min at room temperature and then were subsequently incubated for 30 min in 10% HIFBS at 37°C.

RNA extraction, cDNA synthesis, and quantitative RT-PCR

Total RNA was extracted from isolated hPDL fibroblasts or hPDL explants using Isogen (Nippon Gene, Tokyo, Japan). Total RNA (500 μg) was used to synthesize cDNA with a ReverTra Ace qPCR RT Kit (Toyobo, Osaka, Japan) for quantitative RT-PCR (qRT-PCRs). The mRNA levels encoding each target gene of interest were normalized with glyceraldehyde-3-phosphate dehydrogenase (GAPDH) mRNA in the same samples as housekeeping genes. Data are presented as the fold-change relative to the control group. The primer sequences used in amplification are shown in Supplemental Table S1.

In vivo experimental tooth movement

In total, 15 male 8-wk-old Institute of Cancer research (ICR; Sutton, United Kingdom) mice were used. After anesthetizing the mice with an intraperitoneal injection of isoflurane (10 g/kg), the OTM appliances were set and adjusted as previously described (12). In brief, nickel-titanium coiled springs were activated in order to deliver an orthodontic force of 10 g for 24 h. All experimental protocols were approved by Okayama University's Committee on Use and Care of Animals (OKU-2018697). Sample preparation and hematoxylin and eosin (HE) staining of the distobuccal root of maxillary first molar was performed as previously described (12). The quantification of the sclerostin immunoreactivity in PDL were analyzed using ImageJ/Fiji.

Immunofluorescence

For the detection of sclerostin expression, the cells were fixed in 3% paraformaldehyde, permeabilized in PBS containing 0.5% saponin (MilliporeSigma) for 10 min, and incubated with the primary antibody, rabbit polyclonal anti-sclerostin (dilution, 1:200; Abcam, Cambridge, United Kingdom) in PBS containing 1% bovine serum albumin for

24 h at 4°C followed by species-matched Alexa Fluor 488–conjugated secondary antibody (Thermo Fisher Scientific). Subsequently, Texas Red phalloidin for actin cytoskeleton and Hoechst 33242 (MilliporeSigma) for cell nuclei were stained. The sections were incubated with goat anti-sclerostin (R&D Systems, Minneapolis, MN, USA), followed by species-matched Alexa Fluor 488–conjugated secondary antibody. Nuclei were stained using DAPI (MilliporeSigma). Images were acquired using a confocal laser scanning microscope (FluoView FV500; Olympus).

Statistical analyses

The data of the signal features were presented as the means ± SEM, and other data were presented as the means ± SD. The data were analyzed using either a paired or unpaired Student's *t* test and a 1-way ANOVA followed by Fisher's Least Significant Difference (LSD) test. For Moran's *I*, the paired data were analyzed using Wilcoxon's signed-rank test. The previously mentioned statistical analyses were performed using either the GraphPad Prism 6 software program (GraphPad Software, La Jolla, CA, USA) or the *R* software program (*https://www.R-project.org/*). Measurements at $P < 0.05$ were considered statistically significant.

RESULTS

Ex vivo observation of MS-induced $[Ca^{2+}]_i$ responses in hPDL explants

Figure 1*A* is a schematic illustration showing the continuous compressive force to the intact hPDL explant system. We clearly detected single Fluo8-loaded optical slices of the hPDL explants (Fig. 1*B*). After exposure to MS, a cell (cell 1) responded with a sudden increase in the $[Ca^{2+}]_i$, which was followed by a subsequent decrease to the baseline level (Fig. 1*C–E* and Supplemental Movie S1). Quantifying the $[Ca^{2+}]_i$ uptake showed that the percentage of responsive cells was significantly increased compared with the static group

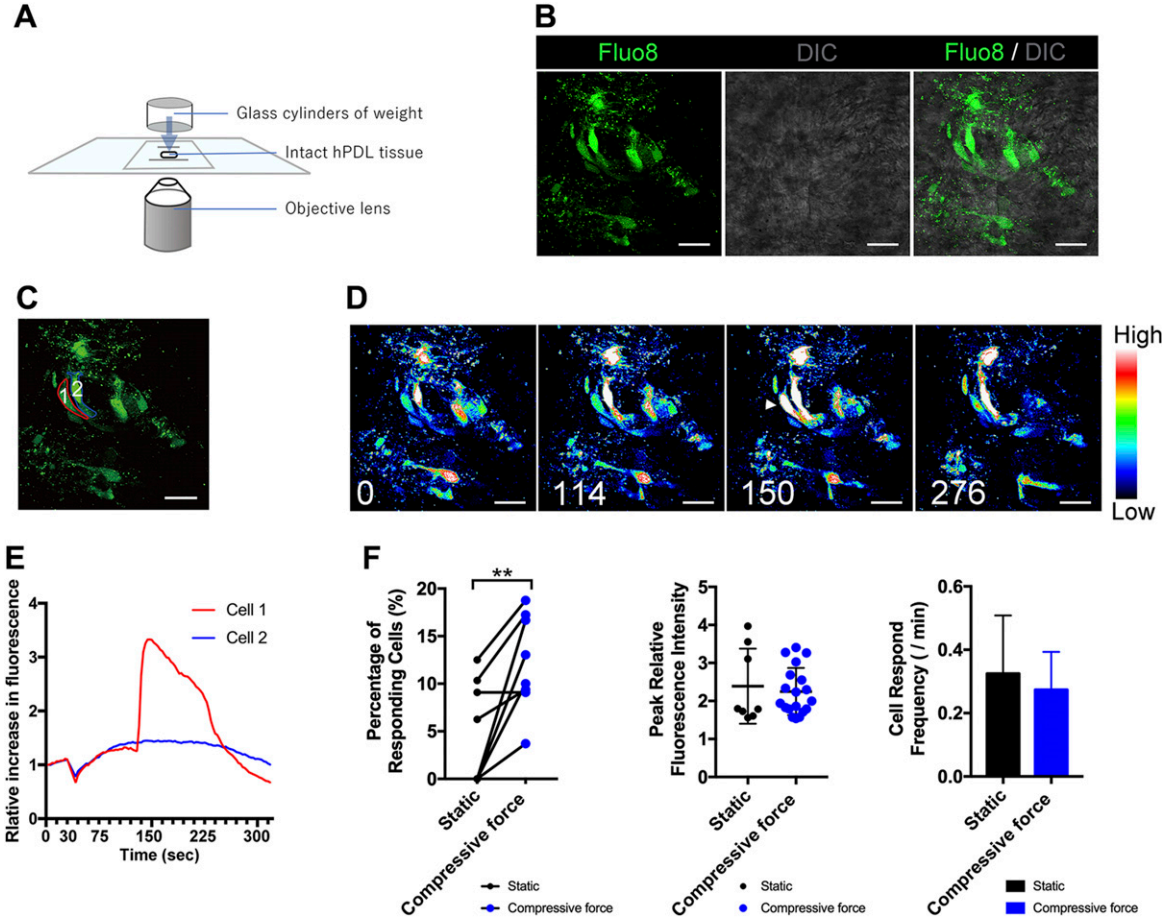

Figure 1. Continuous compressive force–induced $[Ca^{2+}]_i$ responses in human fibroblasts in intact PDL explants. *A*) Schematic diagram of the delivery of continuous compressive force to intact hPDL explants. *B*) The double-labeled fluorescence and interference contrast microscope (DIC) images of hPDL fibroblasts in intact explants tagged with Fluo8 (green). *C*) Individual color lines represent the cells. *D*) Serial pseudocolor images of the hPDL fibroblasts in *B* at 0, 114, 150, and 276 s after the initiation of monitoring. The vertical color scale represents relative fluorescence intensity. Arrowhead indicates $[Ca^{2+}]_i$ response. A movie of the serial pseudocolor images can also be seen in the supplemental data (Supplemental Video S1). *E*) Representative traces of $[Ca^{2+}]_i$ dynamics in individual hPDL fibroblasts in intact explants following continuous compressive force. The elevation of the relative fluorescence intensity was defined by the mean intensity observed before the application of compressive force. *F*) The percentage of responsive cells, peak relative fluorescence intensity in the responsive cells, and cell response frequency in the responsive cells after the continuous compressive force was calculated. The data are expressed as the means ± SD. Scale bars, 20 μm. The asterisks indicate significant differences; $^{**}P < 0.01$: paired Student's *t* test.

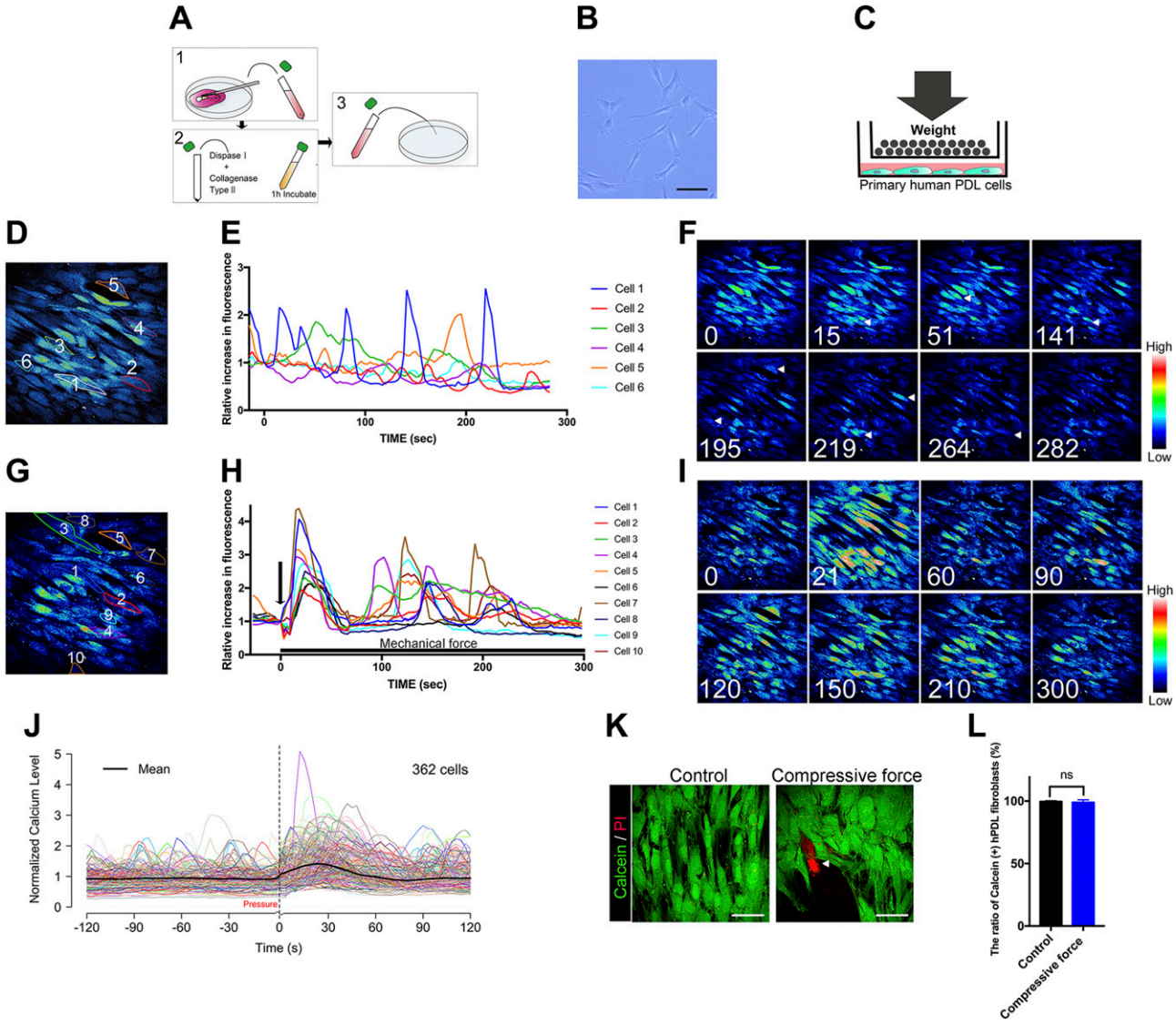

Figure 2. Time-lapse images of the autonomic and continuous compressive force–induced $[Ca^{2+}]_i$ responses in isolated hPDL fibroblasts. *A*) Schematic diagram showing the isolation procedure of primary hPDL fibroblasts. *B*) The primary hPDL fibroblasts 3 d after isolation. *C*) Schematic diagram of the delivery of continuous compressive force to the cells. *D*) Pseudocolor images of the fluorescence-labeled hPDL fibroblasts. The numbered cells represent the cells described in plot *E*. *E*) Representative traces of $[Ca^{2+}]_i$ dynamics in individual hPDL fibroblasts under static conditions. Each color trace indicates the time course of the $[Ca^{2+}]_i$ response of the individual cell represented with the same color. *F*) Serial pseudocolor images of the fluorescence-labeled hPDL fibroblasts taken at 0, 15, 51, 141, 195, 219, and 282 s after the initiation of monitoring. The vertical color scale reflects the relative fluorescence intensity. A movie of the serial pseudocolor images can also be seen in the supplemental data (Supplemental Video S2). *G*) Fluorescence pseudocolor images of the hPDL fibroblasts' response to continuous compressive force. The numbers coded to each cell indicate the cells represented in plot *H*. *H*) Representative traces of $[Ca^{2+}]_i$ dynamics in individual hPDL fibroblasts in response to the continuous compressive force. The elevation of the relative fluorescence intensity was defined by the mean intensity observed before the application of compressive force. Individual color lines of plot in *H* represent the $[Ca^{2+}]_i$-responsive hPDL fibroblasts in the corresponding plot in *G*. *I*) Sequential images of the hPDL fibroblasts taken at 0, 21, 60, 90, 120, 150, 210, and 300 s during the application of MS. A movie of the serial pseudocolor images can also be seen in the supplemental data (Supplemental Video S3). *J*) The $[Ca^{2+}]_i$ profile of all investigated hPDL cells under MS treatment. The average profile is indicated by the block line in black. *K*) Representative fluorescent images of isolated hPDL fibroblasts labeled with calcein or propidium iodide (PI: arrowhead). *L*) Quantification results of hPDL viability tests. All data are expressed as means ± SD. The comparison between control and continuous compressive force groups is determined by unpaired Student's *t* test ($n = 10$ per group). Scale bars, 50 μm.

($P < 0.01$), but statistical significance in terms of the peak relative fluorescence intensity and $[Ca^{2+}]_i$ spark frequencies was not detected (Fig. 1*F*). This might be because of the relatively low sample size of the *ex vivo* experiment using the hPDL explants, which limits the statistical test power of our study.

Isolated hPDL fibroblasts display autonomous $[Ca^{2+}]_i$ responses

Primary hPDL fibroblasts were isolated from freshly extracted teeth and seeded under standard culture conditions (**Fig. 2*A***). A fibroblastic spindle shape and colony

formation were observed on d 3 after the initial plating (Fig. 2*B*). Figure 2*C* is a schematic illustration showing the procedure used to deliver continuous compressive force to primary isolated hPDL fibroblasts. Before investigating the effect of MS on $[Ca^{2+}]_i$ responses, we examined the dynamic of $[Ca^{2+}]_i$ under static conditions. Confocal images of fluorescently labeled representative hPDL fibroblasts showed that some cells displayed autonomic oscillatory $[Ca^{2+}]_i$ activity, with multiple spikes under static conditions during the 300-s experimental period (Fig. 2*D–F* and Supplemental Movie S2).

Continuous compressive force activates the autonomous $[Ca^{2+}]_i$ oscillations in isolated hPDL fibroblasts

We then examined the dynamic of $[Ca^{2+}]_i$ responded to continuous compressive mechanical force. After the application of 2.40 g/cm^2 of continuous compressive force, individual hPDL fibroblasts responded with a sudden elevation of $[Ca^{2+}]_i$ followed by a gradual decline to the baseline level (Fig. 2*G–I* and Supplemental Movie S3). We measured all of the responsive cells in the field of view to avoid biases and calculated the percentage of responsive cells by r_J. The mean $[Ca^{2+}]_i$ profile of all of the observed hPDL fibroblasts (Fig. 2*J* block line in black) was consistent with the examples shown in Fig. 2*H*, in which most hPDL fibroblasts peaked simultaneously (resulting in a sudden increase in the average profile) in response to MS, and the subsequent peaks of each cell occurred at different times (resulting in a flatter average profile). These results suggest that hPDL fibroblasts were transiently sensitized to biomechanical stimuli. Viability assessment showed no differences in the percentages of calcein-positive hPDL fibroblasts between the control or compressive force of 2.40 g/cm^2 for 6-h groups, indicating the static compressive force in this study did not affect cell viability (Fig. 2*K, L*).

Spatiotemporal dynamic of $[Ca^{2+}]_i$ oscillations in response to MS

The spatiotemporal patterns of the $[Ca^{2+}]_i$ response were examined under 2 different magnitudes of compressive force; namely, 0.24 g/cm^2 and 2.40 g/cm^2. As indicated by the heatmap and histograms in **Fig. 3*B–E***, our method of extracting $[Ca^{2+}]_i$ signal features showed an acceptable efficiency for distinguishing the signal pattern of both compression groups from that of the control group. Analyses of $[Ca^{2+}]_i$ signals showed significant increases in the Int, Var, WL, MA, and index *J* after compressive force indicated increased $[Ca^{2+}]_i$ activity of hPDL cells in response to MS at the beginning stage. Although some cells showed a high frequency of signal sparks (see Fig. 3*A* and cell 5 in Fig. 2*H*), most cells showed a decreased frequency of such sparks (see cells 3, 4, and 9 in Fig. 2*H*), thus suggesting a lower mean of MPF in Fig. 3*C, E*. Interestingly, the light compressive force (0.24 g/cm^2) produced lower $[Ca^{2+}]_i$ responses compared with the heavy force (2.40 g/cm^2). The signal feature extraction analysis showed the significant differences in Moran's *I* for MA and index *J* under heavy force, whereas the light force produced no significant difference (Fig. 3*B–E*), indicating that these functions might thus demonstrate a magnitude-dependent behavior in hPDL fibroblasts.

Continuous compressive force biphasically regulates Rankl and Sost expression in isolated hPDL fibroblasts

To clarify the specific underlying role of $[Ca^{2+}]_i$ in the mechanotransduction system of hPDL fibroblasts, we next examined the effect of MS on the profile of the gene expression in relation to bone remodeling. qRT-PCR revealed a significant increase in Rankl, which is associated with the regulation of bone turnover under a compressive force of 2.40 g/cm^2, whereas this expression was decreased under a light compressive force of 0.24 g/cm^2. This biphasic response to compressive MS was also seen in the Sost gene expression. In addition, a significant decrease in the expression of osteoprotegerin (Opg), which occurred in response to compressive force, resulted in a striking mechanical force–dependent increase in the Rankl/Opg ratio (**Fig. 4*A***). These results indicate that continuous compressive force regulates the mRNA levels of factors in hPDL that are known to control bone remodeling.

OTM stimulated the sclerostin expression in compressed PDL

The patterns of sclerostin expression *in vivo* were investigated by experimental OTM in mice. An examination of HE-stained coronal sections confirmed the contraction of the PDL instantaneously after experimental OTM for 24 h (Fig. 4*B*). The OTM stimulated sclerostin expression in the PDL on the compression side (Fig. 4*C* arrowheads). The quantification of sclerostin immunoreactivity in the PDL showed that OTM significantly increased the sclerostin expression on the compression side compared with its tension side or in the control group. (Fig. 4*D*).

Spatiotemporal dynamic of $[Ca^{2+}]_i$ oscillations in response to $[Ca^{2+}]_i$ uptake by A23187

The static compressive force–derived $[Ca^{2+}]_i$ uptake both *in vitro* and *ex vivo* prompted us to investigate the effect on the $[Ca^{2+}]_i$ uptake in hPDL fibroblasts and surrounding bone remodeling. To reveal the possible role of the MS-induced $[Ca^{2+}]_i$ uptake, hPDL fibroblasts were treated with 20 μM A23187, a Ca^{2+}-transporting ionophore, according to a previous study by Resendez *et al*. (28). Ca^{2+} imaging was performed in order to clarify the effect of A23187 on the $[Ca^{2+}]_i$ responses of the hPDL fibroblasts. As expected, A23187 induced a sudden elevation of $[Ca^{2+}]_i$ followed by a maintained plateau phase (**Fig. 5*A–C***). In

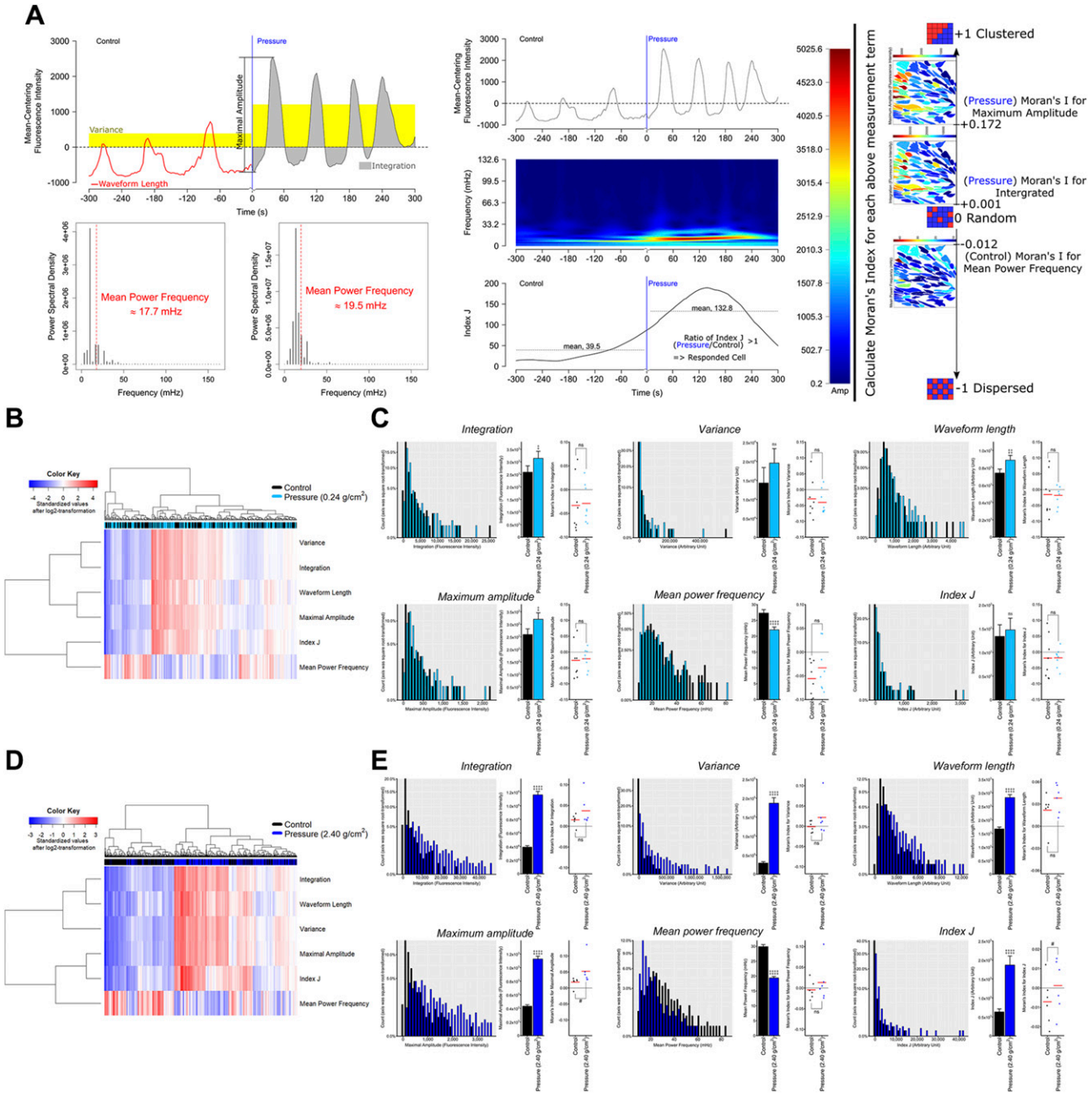

Figure 3. The spatiotemporal dynamic of continuous compressive force–induced $[Ca^{2+}]_i$ signals. *A*) A visualized example for the several feature extraction method of the $[Ca^{2+}]_i$ signal (Var, WL, MA, MPF, and Index *J*) (upper box of middle panel: the original trace of oscillatory wave; middle box of middle panel: the plot of the scaleogram representing the wave transform of original trace; lower box of middle panel: the plot of activity of Index *J* as a function of time). The vertical blue line in the upper and lower boxes marks the starting point of stimulation. Moran's *I* detects the synchronization in the $[Ca^{2+}]_i$ signal with a spatial structure. If neighboring values tend to have similar values, then Moran's *I* would move closer to +1 (indicating a clustered pattern), whereas Moran's *I* would move closer to −1 (indicating a dispersed pattern) if they tend to have dissimilar values. If there is no dependence among them, then Moran's *I* would move closer to 0 (indicating a random pattern) and +1. *B*) The heatmap and cluster analysis of all of the $[Ca^{2+}]_i$ signal features in response to light compressive force. *C*) The $[Ca^{2+}]_i$ signal features and their Moran's *I* in response to light compressive force. *D*) The heatmap and cluster analysis of all of the $[Ca^{2+}]_i$ signal features in response to heavy compressive force. *E*) The $[Ca^{2+}]_i$ signal features and their Moran's *I* in response to heavy compressive force. Ns, not significant. ‡paired Student's *t* test, $^{\#}$Wilcoxon signed-rank test, $^{\ddagger,\ \#}P < 0.05$, $^{\ddagger\ddagger}P < 0.01$, $^{\ddagger\ddagger\ddagger}P < 0.001$, $^{\ddagger\ddagger\ddagger\ddagger}P < 0.0001$.

contrast to the static compressive force–derived $[Ca^{2+}]_i$ uptake, A23187 led to an early peak phase followed by a plateau phase, known as a peak-plateau pattern (Fig. 5*B, D*). As suggested by the heatmap in Fig. 5*E* and histograms in Fig. 5*F*, our signal feature extraction methods again showed satisfactory efficiency for distinguishing the signal pattern of the A23187 group from that of the control group. However, no significant

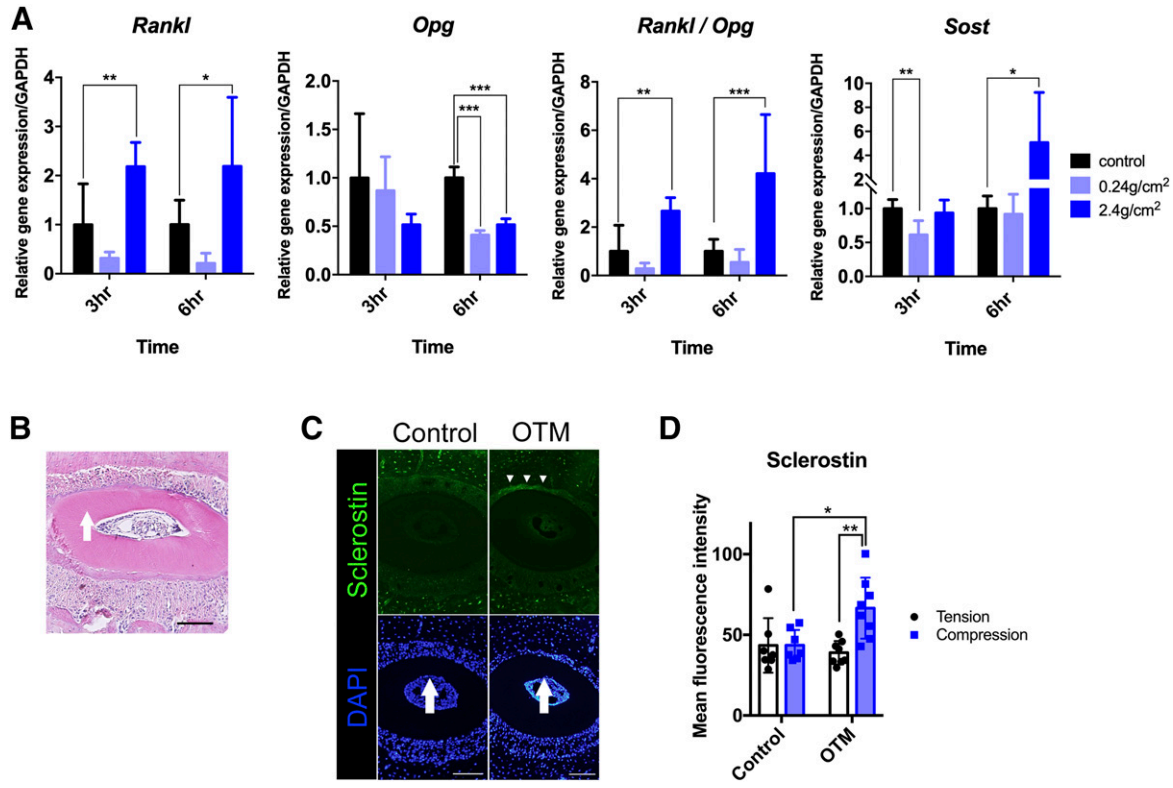

Figure 4. The effect of continuous compressive MS on the gene and protein expression profiles in PDL. *A*) The expression of Rankl, Opg, Rankl/Opg, and Sost in hPDL fibroblasts after exposure to continuous compressive force (0.24 and 2.40 g/cm^2 for 3 and 6 h, respectively). The qRT-PCR results are standardized to the reference gene GAPDH and expressed as the means ± SD from 3 to 9 independent experiments. *B*) The HE staining of the distobuccal root of maxillary first molar. The arrow indicates the direction of orthodontic force. Scale bar, 100μm *C*) Representative images of immunofluorescence staining. The nuclei were stained with DAPI (blue), and sclerostin was stained in green. The arrows indicate the direction of orthodontic force, and the arrowheads indicate the region in which sclerostin signals were detected in PDL. Scale bars, 100 μm. *D*) The sclerostin profile on the compression side and tension side in PDL. An orthodontic force of 10 g was delivered for 24 h. The asterisks indicate significant differences. *$P < 0.05$, **$P < 0.01$, ***$P < 0.001$; a 1-way ANOVA with Fisher's least significant difference test.

differences in Moran's *I* were observed between the control and A23187 group.

All of the signal features showed similar changes after A23187 treatment (Fig. 5*F*) as they had shown following compression pressure treatment (decreased MPF and increased Int, Var, WL, MA, and index *J*), but the heatmap showed that the pattern of $[Ca^{2+}]_i$ activity differed between the compression and A23187 groups (**Fig. 6*A***). Representative histograms also showed that the compression group had significantly higher $[Ca^{2+}]_i$ activity than the A23187 group; however, the percentage of responding cells did not markedly differ between the compression and A23187 groups (Fig. 6*B, C*). A PCA analysis showed a striking difference in the spatiotemporal pattern of $[Ca^{2+}]_i$ response between 2 different magnitudes of compressive MS and treatment with A23187 (Fig. 6*D*).

The $[Ca^{2+}]_i$ uptake by A23187 stimulates Rankl and Sost/sclerostin expression

The A23187-mediated $[Ca^{2+}]_i$ uptake increased the Rankl mRNA expression in a dose- and time-dependent manner, whereas Opg mRNA was not changed, leading to an increase in the ratio of Rankl/Opg (**Fig. 7*A***). This uptake also resulted in increased *Sost* mRNA expression (Fig. 7*B*). Consistent with the *Sost* up-regulation, immunodetection of primary hPDL fibroblasts fixed 6 h after treatment with A23187 showed the increased expression of sclerostin, with punctate stains abundantly visible in cells (Fig. 7*C*). Additionally, intact hPDL explant showed that continuous $[Ca^{2+}]_i$ uptake induced by A23187 resulted in a significant increase in the expression of Rankl, Sost, and Rankl/Opg ratio (Fig. 7*D*). Taken together, these results suggest that the transient augmentation of $[Ca^{2+}]_i$ plays an important role in the biologic responses, which contribute greatly to remodeling activity both in alveolar bone and the PDL itself.

The $[Ca^{2+}]_i$ uptake by A23187 exhibits delayed osteogenic differentiation and mineralization of hPDL fibroblasts

We further examined the effect of A23187 on osteogenic differentiation and mineralization of hPDL fibroblasts. Cells were treated with 2 μM A23187 for 24 h. The qRT-PCR revealed a significant decrease in the

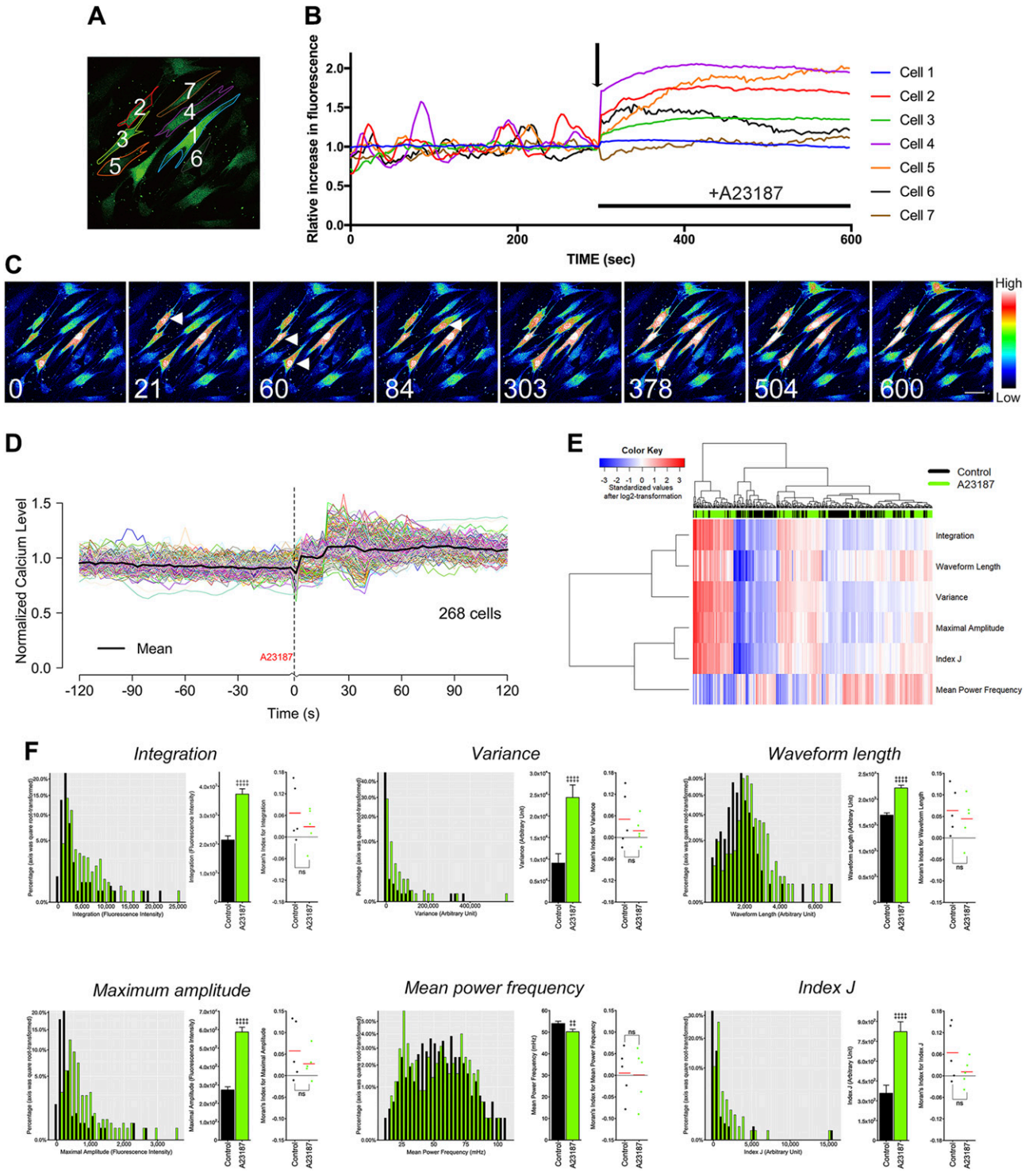

Figure 5. The effect of the A23187-induced $[Ca^{2+}]_i$ uptake on the spatiotemporal cell behavior in hPDL fibroblasts. *A*) Pseudocolor images of the cells after stimulation with 20 μM of A23187. *B*) Representative plot for the numbered cells in *A*. The arrow indicates the initiation of A23187 treatment. *C*) Consecutive images of the A23187-induced $[Ca^{2+}]_i$ uptake in hPDL fibroblasts taken at 0, 21, 60, 84, 303, 378, 504, and 600 s. The arrowheads indicate the $[Ca^{2+}]_i$ response. *D*) The $[Ca^{2+}]_i$ profile of all investigated hPDL cells under A23187 treatment. The average profile is indicated by the block line in black. *E*) The heatmap and cluster analysis of all the $[Ca^{2+}]_i$ signal features. *F*) The $[Ca^{2+}]_i$ signal features and their Moran's *I*. ns, not significant. ‡paired Student's *t* test, #Wilcoxon signed-rank test, ‡, #$P < 0.05$, ‡‡$P < 0.01$, ‡‡‡$P < 0.001$, ‡‡‡‡$P < 0.0001$.

runt-related transcription factor 2 (Runx2) mRNA levels, whereas the Sost and osterix (Osx) expression was stimulated for 24 h, suggesting decreased osteogenic differentiation potential (Fig. 7*E*). In accordance with the mRNA data, the A23187-treated hPDL fibroblasts showed a decelerated onset of mineralized nodule formation, indicating delayed mineralization (Fig. 7*F*).

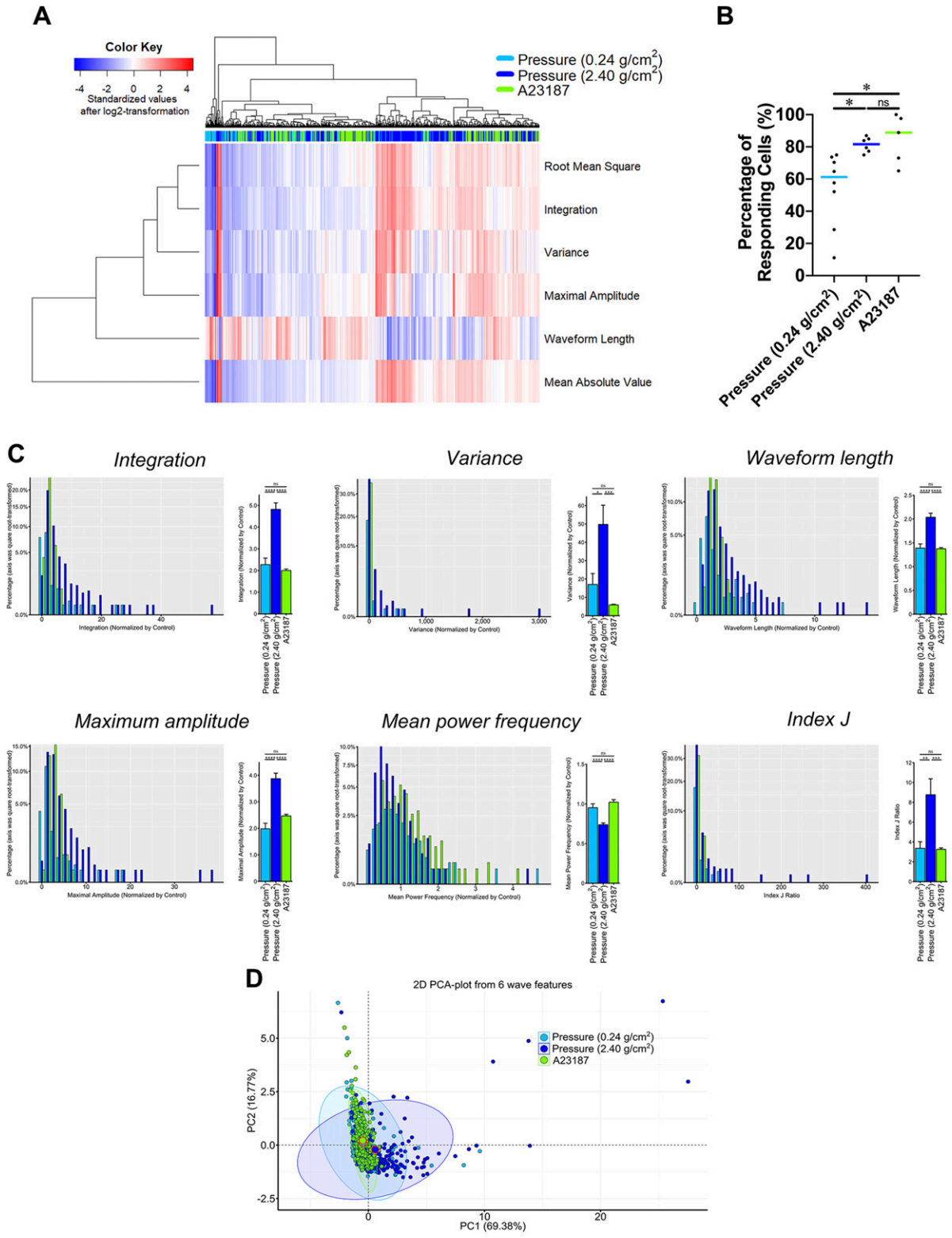

Figure 6. A comparison of the $[Ca^{2+}]_i$ signal features between continuous compressive force and A23187 treatment. *A*) The heatmap and cluster analysis of all of the $[Ca^{2+}]_i$ signal features. *B*) The percentage of responding cells defined by η. *C*) $[Ca^{2+}]_i$ signal features. *D*) A PCA with the best-fitted ellipse of all the $[Ca^{2+}]_i$ signal features. The percentage of explained variation was shown in parentheses. 2D, 2-dimensional; ns, not significant; PC1, first principal component; PC2, second principal component. Asterisk, 1-way ANOVA with Fisher's least significant difference test; $*P < 0.05$, $**P < 0.01$, $***P < 0.001$, $****P < 0.0001$.

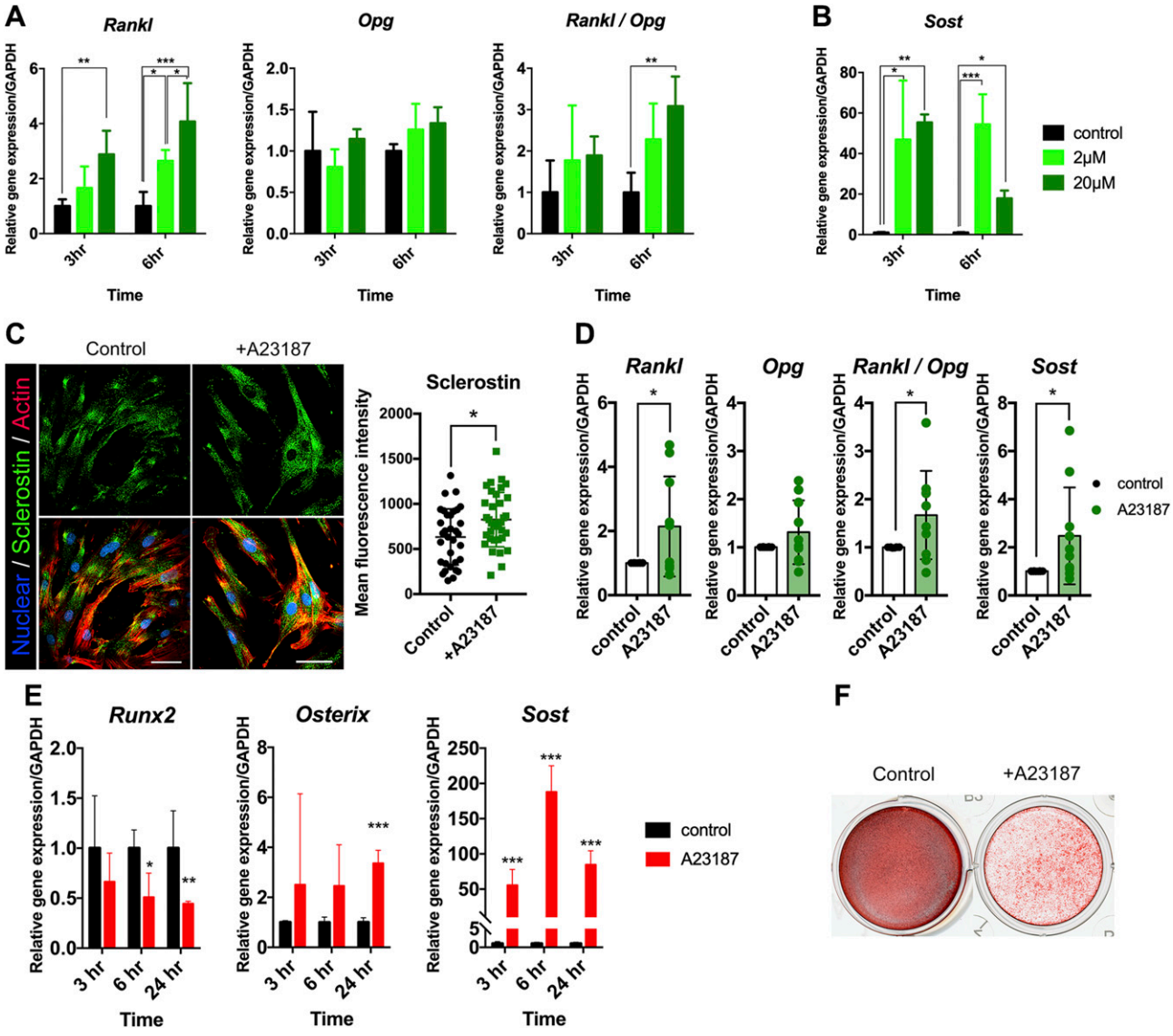

Figure 7. The effect of the A23187-induced $[Ca^{2+}]_i$ uptake on the gene expression profiles and osteogenic differentiation in hPDL fibroblasts. *A*, *B*) The expression of Rankl, Opg, Rankl/Opg, and Sost in hPDL fibroblasts treated with 2 and 20 μM for 3 and 6 h, respectively. *C*) Fluorescence images of hPDL cells showing nuclei (blue), sclerostin (green), and actin (red). Isolated hPDL fibroblasts were treated with A23187 at 20 μM for 6 h. Scale bar, 50 μm. Asterisks indicate significant differences. $*P < 0.05$; unpaired Student's *t* test. *D*) The expression of Rankl, Opg, Rankl/Opg, and Sost in intact hPDL explants treated with 20 μM for 6 h. *E*) The role of Ca^{2+} in osteogenic differentiation and mineralization of hPDL fibroblasts. The Runx2, Osx, and Sost mRNA levels in isolated hPDL fibroblasts treated with 2 μM of A23187. *F*) Alizarin red staining of hPDL fibroblasts after 14 d of osteogenic differentiation. Cells were treated with vehicle or 2 μM A23187. The qRT-PCR results are standardized to the reference gene GAPDH and expressed as the means ± SD. The asterisks indicate significant differences. $*P < 0.05$, $**P < 0.01$, $***P < 0.001$; a 1-way ANOVA with Fisher's least significance difference test in *A* and *B* or unpaired Student's *t* test in *D* and *E*.

Blockade of GJs suppress autonomous and MS-induced $[Ca^{2+}]_i$ responses in hPDL fibroblasts

The behavior of hPDL fibroblasts displayed direct cell-cell communication *via* the functional GJs (20). We determined whether this intercellular network contributes to the $[Ca^{2+}]_i$-based mechanotransduction of hPDL using a GJ inhibitor, 18α-GA. In the static condition, the heatmap (Supplemental Fig. S1*A*) and histograms (Supplemental Fig. S1*B*) showed all the signal features to have significantly decreased except for MPF. These results indicate that the inhibition of GJ suppressed the autonomous $[Ca^{2+}]_i$ responses in hPDL fibroblasts. We next investigated the effect of GJ inhibition on the dynamic of compressive MS–induced $[Ca^{2+}]_i$ signals in both culture fibroblasts and hPDL explants. All of the signal features exhibited the opposite changes compared with the results from compressive MS or A23187 treatment (**Fig. 8*A–D***). The inhibitor also caused a reduction in the responsive cell percentage to compressive MS both in isolated fibroblasts (Fig. 8*C*) and in hPDL explants (Fig. 8*E*).

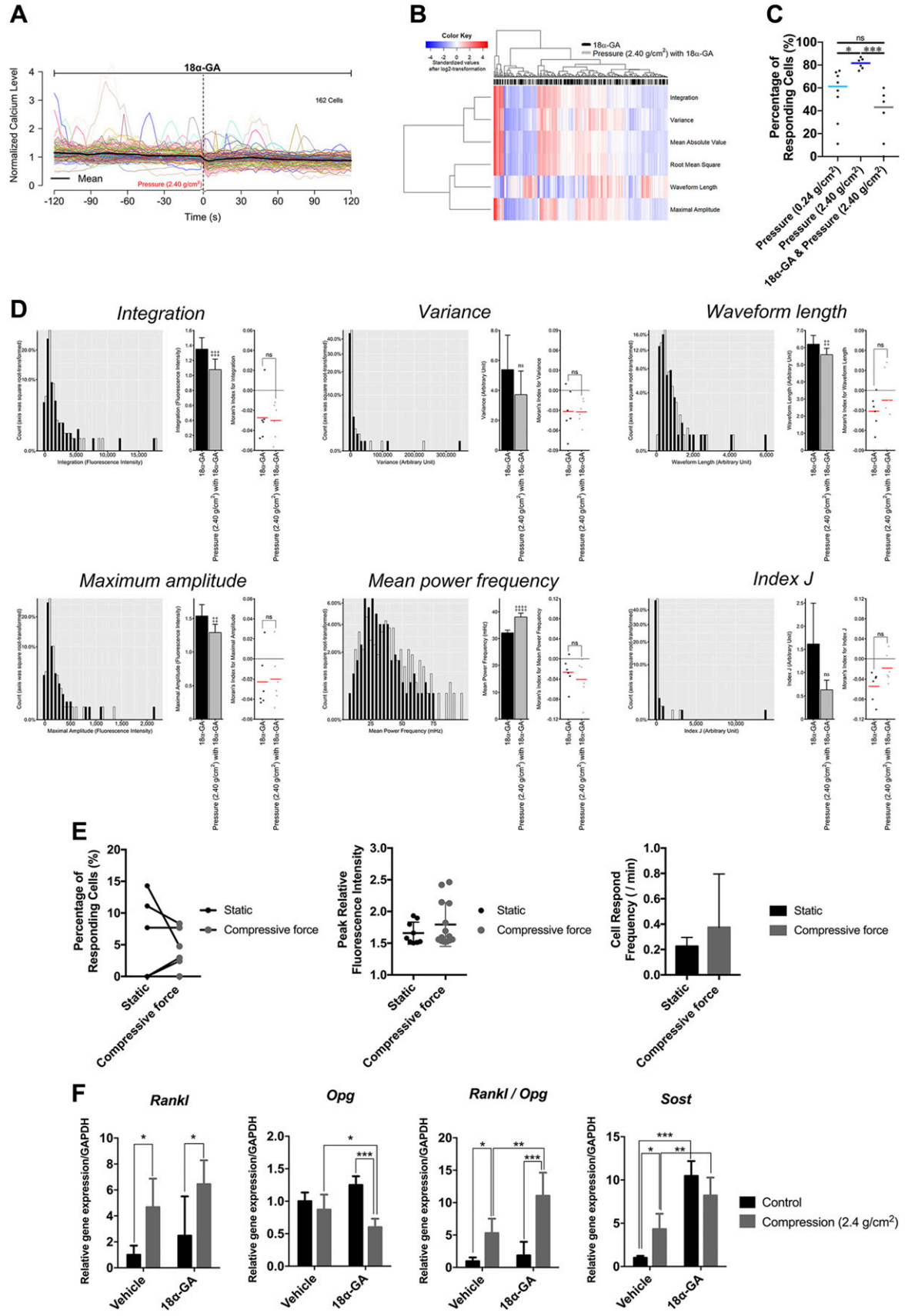

Figure 8. The effect of the blockade of GJ on the dynamic of continuous compressive force–induced $[Ca^{2+}]_i$ signals and gene expression profiles in hPDL. *A*) The $[Ca^{2+}]_i$ profile of all investigated hPDL cells under 18α-GA treatment. The average profile is indicated by the block line in black. *B*) The heatmap and cluster analysis of all of the $[Ca^{2+}]_i$ signal features. *C*) The comparison

(*continued on next page*)

Gap junctional cell-cell communication affects the MS-induced gene regulations involved in bone remodeling

We further evaluated the functional involvement of GJs on compressive MS-induced gene regulations in hPDL fibroblasts. Treatment with 18α-GA displayed a lower Opg mRNA expression in MS-induced hPDL fibroblasts, which led to an increase in the Rankl/Opg ratio (Fig. 8*F*). Furthermore, the inhibitor also resulted in an increased Sost mRNA expression (Fig. 8*F*).

DISCUSSION

The conversion of physical force into biochemical information is fundamental to physiologic functions in the context of living cells and tissue. It is apparent that the PDL exhibits a state of compression that is dependent on the level of tooth-mediated pressure. Importantly, this process relates to the changes in the local microenvironment of the cells residing within the alveolar bone. Previous studies have shown the MS-induced $[Ca^{2+}]_i$ uptake in hPDL fibroblasts (16); however, a comprehensive review of the importance of $[Ca^{2+}]_i$ and its relevance to the mechanotransduction that underlies bone remodeling around the teeth is yet to be established. The present study demonstrates the behavior and connectivity of the $[Ca^{2+}]_i$ dynamic in the mechanotranduction system of hPDL fibroblasts and examines the expression of biologic mediators in order to determine the molecular basis of the observed changes.

The natural environment of cells is 3-dimensional, which differs from *in vitro* 2-dimensional cultures. The $[Ca^{2+}]_i$ responses of PDL fibroblasts has been demonstrated using traditional cell culture models in a previous report by Nakago-Matsuo *et al*. (16). However, whether similar $[Ca^{2+}]_i$ responses are produced in the cells in integrated PDL tissues is unclear because the complexity of the 3D-dimensional microenvironment is lost *in vitro*. This study highlights a novel *ex vivo* platform that facilitates real-time $[Ca^{2+}]_i$ monitoring of hPDL fibroblasts in response to continuous compressive force. Our findings from these experiments clearly show that hPDL is truly mechanosensitive at the cellular level within intact tissue. Another noteworthy finding of the live-cell Ca^{2+} imaging system is that some hPDL fibroblasts triggered $[Ca^{2+}]_i$ oscillations even under static conditions. Previous studies showed that autonomic $[Ca^{2+}]_i$ oscillations could be visualized in bovine articular chondrocytes (29) as well as in osteoblasts and osteocytes within the bone tissue (21, 30). To our knowledge, the present study may be the first to describe physiologic autonomic $[Ca^{2+}]_i$ oscillations in hPDL fibroblasts.

The spatiotemporal dynamic of hPDL fibroblasts showed that all of the signal features except for the MPF significantly increased in response to both the different magnitudes of compressive MS and A23187 exposure. These results indicate that the different magnitudes of MS influence the behavior of $[Ca^{2+}]_i$ activities, which may profoundly affect the biologic role of hPDL fibroblasts. Not only the amplitude of the $[Ca^{2+}]_i$ elevations but also the period or frequency of the $[Ca^{2+}]_i$ oscillations are coded by MS (31). Similar to a previous report on osteoblasts by Meng *et al*. (32), we observed 2 major patterns of $[Ca^{2+}]_i$ activity after compressive MS. After the early increased $[Ca^{2+}]_i$ signal spark, the first type is followed by the suppressed frequency of the signal spark (see cells 3, 4, and 9 in Fig. 2*H*), whereas the second type is followed by the increased frequency of the signal spark (see Fig. 3*A* and cell 5 in Fig. 2*H*).

The increased Moran's *I* for MA and Index *J* suggested increased synchronization of $[Ca^{2+}]_i$ activity among hPDL cells under a compressive force of 2.40 g/cm^2 (Fig. 3*D, E*). This is consistent with the findings shown in Fig. 2*J*, which indicate that the desynchronization of $[Ca^{2+}]_i$ activity results in a very flat average profile (see the block line in black from −120 to 0 s in Fig. 2*J*), and increased synchronization of $[Ca^{2+}]_i$ activity results in a slightly twisted average profile (see the block line in black from 75 to 120 s in Fig. 2*J*). Taken together, these findings suggest that the compression pressure might affect the pattern of cell-cell communication among hPDL cells (20, 33).

On the other hand, A23187 induces a totally different peak-plateau pattern in the $[Ca^{2+}]_i$ activity (Fig. 5*B, D*), and Moran's *I* (Fig. 5*F*) suggests that A23187 simply rose the $[Ca^{2+}]_i$ level without inducing any changes in cell-cell communication. This indicates that gap junctional intercellular communication in primary hPDL cells is not influenced by A23187, but it is influenced by MS. Indeed, 18α-GA interrupts the heavy force–induced synchronization of $[Ca^{2+}]_i$ as shown by Moran's *I* (Figs. 3*E* and 8*D*), which is consistent with a previous report on hepatocytes by Tordjmann *et al*. (34). This suggests that the other signaling pathways, including paracrine communication and ATP, may also induce hPDL cells to synchronize the MS-induced signals (35). Multiple patterns of $[Ca^{2+}]_i$ have been reported to be induced by physical and biochemical stimuli in other cell types (*e.g.*, Hela cells and osteoblasts) (32, 36). Nevertheless, the causality of these multiple $[Ca^{2+}]_i$ patterns remains unclear. Our findings from a PCA analysis indicate the existence of heterogeneity in hPDL cells when they respond to stimuli and other treatments (Fig. 6*D*), which may contribute to the differences of gene

in the percentage of responding cells defined by r_J. *D*) [Ca2+]$_i$ signal features. Ns, not significant. ‡paired Student's *t* test. ‡$P < 0.05$, ‡‡$P < 0.01$, ‡‡‡$P < 0.001$, ‡‡‡‡$P < 0.0001$. *E*) The percentage of responsive cells, peak relative fluorescence intensity in the responsive cells, and cell response frequency in the responsive cells after the continuous compressive force was calculated. The intact hPDL explants were treated with 30 μM of 18α-GA for 6 h prior to the experiments. *F*) The expression of Rankl, Opg, Rankl/Opg, and Sost in hPDL fibroblasts treated with 5.0 μM of 18α-GA for 6 h. The qRT-PCR results are standardized to the reference gene GAPDH and expressed as the means ± SD. The asterisks indicate significant differences. *$P < 0.05$, **$P < 0.01$, ***$P < 0.001$; a 1-way ANOVA with Fisher's least significant difference test.

expression indicated by the qRT-PCR results (Figs. 4*A*, 7*A*, *B*, *D*, and 8*F*). However, the precise mechanism that caused this heterogeneity and which downstream functions this heterogeneity impact remains to be elucidated. The answer to these questions is worthy of further study because this might help to identify novel functions of PDL cells.

The qRT-PCR results determined that the mechanical signals involved in mechanotransuduction pathway regulate the Rankl, Sost, and Rankl/Opg expression in hPDL fibroblasts. This regulatory function of gene expression under compressive conditions was consistent with the previously described results (12). Furthermore, the A23187-induced transient and continuous $[Ca^{2+}]_i$ uptake also led to the increased expression of Rankl and Sost/sclerostin, indicating that Ca^{2+} is a potent physiologic inducer that initiates bone remodeling. Many studies have explored the importance of the information contained in the $[Ca^{2+}]_i$ signal and its molecular regulation (37–39). The human gingival fibroblasts responded to tensile MS by a unique $[Ca^{2+}]_i$ signaling pattern, which is the initial rapid Ca^{2+} transient and subsequent slow oscillations with a large amplitude (15). Such large amplitude increases of $[Ca^{2+}]_i$ may be necessary for the spatially appropriate filamentous actin rearrangement at the force transfer sites (40). The signals of tensile MS in hPDL fibroblasts down-regulate Rankl (41, 42) while also expressing osteoblastic characteristics, thereby influencing both the osteogenic differentiation and mineralization processes (43). The role of $[Ca^{2+}]_i$ in bone is also supported by the recent findings that fluid flow–induced Ca^{2+} oscillations influence extracellular vesicles containing bone regulatory proteins released in osteocytes, suggesting a critical role for $[Ca^{2+}]_i$-mediated signaling in bone adaptation (44). We found that compressive MS mediated a sudden elevation of $[Ca^{2+}]_i$ followed by a gradual decline to the baseline level, whereas A23187 induced a sudden elevation of $[Ca^{2+}]_i$ followed by a maintained plateau phase in primary hPDL fibroblasts. Consistent with these variations in $[Ca^{2+}]_i$ mobilization patterns detected on live-cell imaging analyses, we showed different Opg expressions, suggesting that the biologic regulation *via* $[Ca^{2+}]_i$ signaling differs to some extent between compressive MS– and A23187-induced stimulation in hPDL fibroblasts. These findings suggest that the local mechanotransduction system of hPDL fibroblasts is closely correlated with the differential response to different types of MS in bone remodeling. However, the detailed mechanism underlying how hPDL fibroblasts distinguish the independent behavior of $[Ca^{2+}]_i$ signals remains unclear and should be explored in a future study.

We further showed that the treatment of A23187 suppressed alizarin red positive reaction and regulated the gene expression of osteoblastic differentiation. PDL cells have been shown to possess osteoblastic phenotypes for the continued remodeling of alveolar bone (45), and osteoblasts transduce mechanical stimuli into biochemical signals *via* intracellular signaling cascades, including the Wnt (46), GTPase (47), and Ca^{2+} pathways (48). Wnt/β-catenin signaling plays a key role in osteogenesis by promoting the osteoblastic differentiation and mineralization, and Sost/sclerostin has been reported to mediate mechanical cues in bone by antagonizing Wnt/β-catenin signaling (49, 50). Past studies suggested that Osx has the ability to modulate Sost/sclerostin *via* a negative feedback loop of bone formation through Wnt (51, 52). As a result, in our study, A23187-induced Sost/sclerostin up-regulation might be coordinated by the Osx, which is consistent with the previous study (52). Osx is also thought to function as a downstream target of Runx2, and it is essential for the differentiation of preosteoblasts into immature osteoblasts (53). However, the Osx expression is regulated by both Runx2-dependent and -independent mechanisms (54). Our results suggest that the increased levels of Osx mRNA expression in this study is Runx2-independent. These findings together with the data regarding a delayed alizarin red positive reaction suggest that the $[Ca^{2+}]_i$ uptake in hPDL fibroblasts may be attributed to bone remodeling, which occurs concurrently with mineralization.

In summary, the present study demonstrates for the first time that MS-induced $[Ca^{2+}]_i$ oscillations and transients can occur in integral hPDL tissue. The results of our study suggest an important role for augmented MS-mediated $[Ca^{2+}]_i$ signaling in hPDL at compression sites of bone remodeling (**Fig. 9**). This coordination of $[Ca^{2+}]_i$ signaling may have important consequences for the

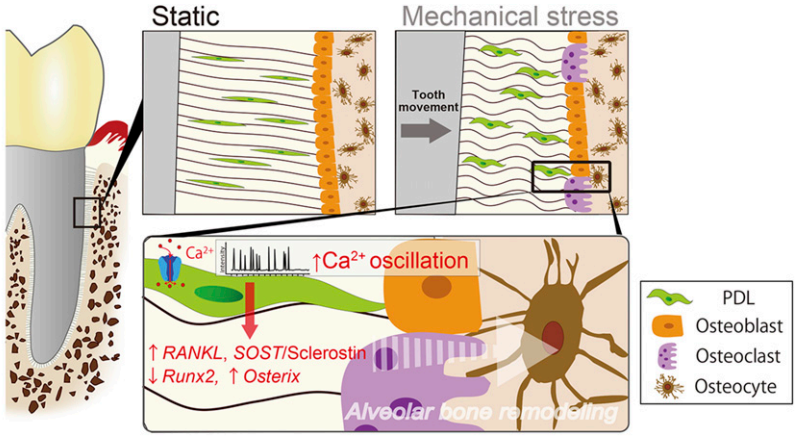

Figure 9. Schematic model depicting the role of $[Ca^{2+}]_i$-based mechanotransduction in hPDL fibroblasts. Shown is the concluding summary diagram of this study. First, our findings suggest that tooth movement–driven compressive force was induced in hPDL fibroblasts, resulting in the activation of autonomous $[Ca^{2+}]_i$ oscillations. Second, our findings collectively suggest that the MS-induced $[Ca^{2+}]_i$ uptake stimulates Sost/sclerostin and Osx and suppresses Runx2, thereby reducing bone formation. Simultaneously, this also induces an increase in the production of Rankl by the hPDL, leading to the stimulation of osteoclastic bone resorption.

PDL function, raising the possibility that Rankl/Opg and canonical Wnt/β-catenin signaling are involved as early signaling processes in tooth movement–initiated bone remodeling. FJ

ACKNOWLEDGMENTS

The present work was supported by Grant-in-Aid for Scientific Research [to Y.I. (17H04413) and H.K. (19H03859)] from the Japan Society for the Promotion of Science, Japan. The authors declare no conflicts of interest.

AUTHOR CONTRIBUTIONS

Y. Ishihara designed the study; E. Ei Hsu Hlaing, Y. Ishihara, and Z. Wang wrote the manuscript; E. Ei Hsu Hlaing, Y. Ishihara, and N. Odagaki conducted the study; E. Ei Hsu Hlaing, Y. Ishihara, and Z. Wang analyzed the data; Y. Ishihara, Z. Wang, and H. Kamioka interpreted the data and approved the final version of the manuscript; and Y. Ishihara is responsible for the integrity of the data analysis.

REFERENCES

1. Turner, C. H., and Pavalko, F. M. (1998) Mechanotransduction and functional response of the skeleton to physical stress: the mechanisms and mechanics of bone adaptation. *J. Orthop. Sci.* **3**, 346–355
2. McCulloch, C. A., Lekic, P., and McKee, M. D. (2000) Role of physical forces in regulating the form and function of the periodontal ligament. *Periodontol. 2000* **24**, 56–72
3. Pavasant, P., and Yongchaitrakul, T. (2011) Role of mechanical stress on the function of periodontal ligament cells. *Periodontol. 2000* **56**, 154–165
4. Nayak, B. N., Galil, K. A., Wiltshire, W., and Lekic, P. C. (2013) Molecular biology of orthodontic tooth movement. *J. Dent. Oral Health.* **1**, 1–6
5. Somjen, D., Binderman, I., Berger, E., and Harell, A. (1980) Bone remodelling induced by physical stress is prostaglandin E2 mediated. *Biochim. Biophys. Acta* **627**, 91–100
6. Davidovitch, Z., Nicolay, O. F., Ngan, P. W., and Shanfeld, J. L. (1988) Neurotransmitters, cytokines, and the control of alveolar bone remodeling in orthodontics. *Dent. Clin. North Am.* **32**, 411–435
7. Naruse, K., and Sokabe, M. (1993) Involvement of stretch-activated ion channels in Ca^{2+} mobilization to mechanical stretch in endothelial cells. *Am. J. Physiol.* **264**, C1037–C1044
8. Manokawinchoke, J., Limjeerajarus, N., Limjeerajarus, C., Sastravaha, P., Everts, V., and Pavasant, P. (2015) Mechanical force-induced TGFB1 increases expression of SOST/POSTN by hPDL cells. *J. Dent. Res.* **94**, 983–989
9. Nakao, K., Goto, T., Gunjigake, K. K., Konoo, T., Kobayashi, S., and Yamaguchi, K. (2007) Intermittent force induces high RANKL expression in human periodontal ligament cells. *J. Dent. Res.* **86**, 623–628
10. Yamaguchi, M. (2009) RANK/RANKL/OPG during orthodontic tooth movement. *Orthod. Craniofac. Res.* **12**, 113–119
11. Li, Y., Zheng, W., Liu, J. S., Wang, J., Yang, P., Li, M. L., and Zhao, Z. H. (2011) Expression of osteoclastogenesis inducers in a tissue model of periodontal ligament under compression. *J. Dent. Res.* **90**, 115–120
12. Odagaki, N., Ishihara, Y., Wang, Z., Ei Hsu Hlaing, E., Nakamura, M., Hoshijima, M., Hayano, S., Kawanabe, N., and Kamioka, H. (2018) Role of osteocyte-PDL crosstalk in tooth movement via SOST/sclerostin. *J. Dent. Res.* **97**, 1374–1382
13. Berridge, M. J., Bootman, M. D., and Lipp, P. (1998) Calcium–a life and death signal. *Nature* **395**, 645–648
14. Rubin, J., Rubin, C., and Jacobs, C. R. (2006) Molecular pathways mediating mechanical signaling in bone. *Gene* **367**, 1–16
15. Arora, P. D., Bibby, K. J., and McCulloch, C. A. (1994) Slow oscillations of free intracellular calcium ion concentration in human fibroblasts responding to mechanical stretch. *J. Cell. Physiol.* **161**, 187–200
16. Nakago-Matsuo, C., Matsuo, T., and Nakago, T. (1996) Intracellular calcium response to hydraulic pressure in human periodontal ligament fibroblasts. *Am. J. Orthod. Dentofacial Orthop.* **109**, 244–248
17. Lekic, P., and McCulloch, C. A. (1996) Periodontal ligament cell population: the central role of fibroblasts in creating a unique tissue. *Anat. Rec.* **245**, 327–341
18. Kawanabe, N., Murata, S., Murakami, K., Ishihara, Y., Hayano, S., Kurosaka, H., Kamioka, H., Takano-Yamamoto, T., and Yamashiro, T. (2010) Isolation of multipotent stem cells in human periodontal ligament using stage-specific embryonic antigen-4. *Differentiation* **79**, 74–83
19. Ishihara, Y., Sugawara, Y., Kamioka, H., Kawanabe, N., Hayano, S., Balam, T. A., Naruse, K., and Yamashiro, T. (2013) Ex vivo real-time observation of Ca(2+) signaling in living bone in response to shear stress applied on the bone surface. *Bone* **53**, 204–215
20. Kato, R., Ishihara, Y., Kawanabe, N., Sumiyoshi, K., Yoshikawa, Y., Nakamura, M., Imai, Y., Yanagita, T., Fukushima, H., Kamioka, H., Takano-Yamamoto, T., and Yamashiro, T. (2013) Gap-junction-mediated communication in human periodontal ligament cells. *J. Dent. Res.* **92**, 635–640
21. Ishihara, Y., Sugawara, Y., Kamioka, H., Kawanabe, N., Kurosaka, H., Naruse, K., and Yamashiro, T. (2012) In situ imaging of the autonomous intracellular $Ca^{(2+)}$ oscillations of osteoblasts and osteocytes in bone. *Bone* **50**, 842–852
22. Kanzaki, H., Chiba, M., Shimizu, Y., and Mitani, H. (2002) Periodontal ligament cells under mechanical stress induce osteoclastogenesis by receptor activator of nuclear factor kappaB ligand up-regulation via prostaglandin E2 synthesis. *J. Bone Miner. Res.* **17**, 210–220
23. Sternberg, S. R. (1983) Biomedical image processing. *Computer* **16**, 22–34
24. Phinyomark, A., Thongpanja, S., Phukpattaranont, P., and Limsakul, C. (2012) The usefulness of mean and median frequencies in electromyography analysis. In *Computational Intelligence in Electromyography Analysis - A Perspective on Current Applications and Future Challenges* (Naik, G. R., ed.), pp. 195–220, InTech, Rijeka, Croatia
25. Chowdhury, R. H., Reaz, M. B., Ali, M. A., Bakar, A. A., Chellappan, K., and Chang, T. G. (2013) Surface electromyography signal processing and classification techniques. *Sensors (Basel)* **13**, 12431–12466
26. Ruffinatti, F. A., Lovisolo, D., Distasi, C., Ariano, P., Erriquez, J., and Ferraro, M. (2011) Calcium signals: analysis in time and frequency domains. *J. Neurosci. Methods* **199**, 310–320
27. Moran, P. A. (1950) Notes on continuous stochastic phenomena. *Biometrika* **37**, 17–23
28. Resendez, E., Jr., Ting, J., Kim, K. S., Wooden, S. K., and Lee, A. S. (1986) Calcium ionophore A23187 as a regulator of gene expression in mammalian cells. *J. Cell Biol.* **103**, 2145–2152
29. Yellowley, C. E., Jacobs, C. R., Li, Z., Zhou, Z., and Donahue, H. J. (1997) Effects of fluid flow on intracellular calcium in bovine articular chondrocytes. *Am. J. Physiol.* **273**, C30–C36
30. Jing, D., Baik, A. D., Lu, X. L., Zhou, B., Lai, X., Wang, L., Luo, E., and Guo, X. E. (2014) In situ intracellular calcium oscillations in osteocytes in intact mouse long bones under dynamic mechanical loading. *FASEB J.* **28**, 1582–1592
31. Godbout, C., Follonier Castella, L., Smith, E. A., Talele, N., Chow, M. L., Garonna, A., and Hinz, B. (2013) The mechanical environment modulates intracellular calcium oscillation activities of myofibroblasts. *PLoS One* **8**, e64560
32. Meng, G., Li, C., Sun, H., and Lee, I. (2018) Multiple calcium patterns of rat osteoblasts under fluidic shear stress. *J. Orthop. Res.* **36**, 2039–2051
33. Su, M., Borke, J. L., Donahue, H. J., Li, Z., Warshawsky, N. M., Russell, C. M., and Lewis, J. E. (1997) Expression of connexin 43 in rat mandibular bone and periodontal ligament (PDL) cells during experimental tooth movement. *J. Dent. Res.* **76**, 1357–1366
34. Tordjmann, T., Berthon, B., Claret, M., and Combettes, L. (1997) Coordinated intercellular calcium waves induced by noradrenaline in rat hepatocytes: dual control by gap junction permeability and agonist. *EMBO J.* **16**, 5398–5407
35. Wyles, S. P., Hrstka, S. C., Reyes, S., Terzic, A., Olson, T. M., and Nelson, T. J. (2016) Pharmacological modulation of calcium homeostasis in familial dilated cardiomyopathy: an in vitro analysis from an RBM20 patient-derived iPSC model. *Clin. Transl. Sci.* **9**, 158–167

36. Morita, M., Nakane, A., Fujii, Y., Maekawa, S., and Kudo, Y. (2015) High cell density upregulates calcium oscillation by increasing calcium store content via basal mitogen-activated protein kinase activity. *PLoS One* **10**, e0137610
37. Dolmetsch, R. E., Xu, K., and Lewis, R. S. (1998) Calcium oscillations increase the efficiency and specificity of gene expression. *Nature* **392**, 933–936
38. You, J., Reilly, G. C., Zhen, X., Yellowley, C. E., Chen, Q., Donahue, H. J., and Jacobs, C. R. (2001) Osteopontin gene regulation by oscillatory fluid flow via intracellular calcium mobilization and activation of mitogen-activated protein kinase in MC3T3-E1 osteoblasts. *J. Biol. Chem.* **276**, 13365–13371
39. Wiederkehr, A., Szanda, G., Akhmedov, D., Mataki, C., Heizmann, C. W., Schoonjans, K., Pozzan, T., Spät, A., and Wollheim, C. B. (2011) Mitochondrial matrix calcium is an activating signal for hormone secretion. *Cell Metab.* **13**, 601–611
40. Glogauer, M., Arora, P., Yao, G., Sokholov, I., Ferrier, J., and McCulloch, C. A. (1997) Calcium ions and tyrosine phosphorylation interact coordinately with actin to regulate cytoprotective responses to stretching. *J. Cell Sci.* **110**, 11–21
41. Kook, S. H., Jang, Y. S., and Lee, J. C. (2011) Human periodontal ligament fibroblasts stimulate osteoclastogenesis in response to compression force through TNF-α-mediated activation of CD4+ T cells. *J. Cell. Biochem.* **112**, 2891–2901
42. Li, S., Zhang, H., Li, S., Yang, Y., Huo, B., and Zhang, D. (2015) Connexin 43 and ERK regulate tension-induced signal transduction in human periodontal ligament fibroblasts. *J. Orthop. Res.* **33**, 1008–1014
43. Wescott, D. C., Pinkerton, M. N., Gaffey, B. J., Beggs, K. T., Milne, T. J., and Meikle, M. C. (2007) Osteogenic gene expression by human periodontal ligament cells under cyclic tension. *J. Dent. Res.* **86**, 1212–1216
44. Morrell, A. E., Brown, G. N., Robinson, S. T., Sattler, R. L., Baik, A. D., Zhen, G., Cao, X., Bonewald, L. F., Jin, W., Kam, L. C., and Guo, X. E. (2018) Mechanically induced Ca^{2+} oscillations in osteocytes release extracellular vesicles and enhance bone formation. *Bone Res.* **6**, 6
45. Roberts, W. E., Mozsary, P. G., and Klingler, E. (1982) Nuclear size as a cell-kinetic marker for osteoblast differentiation. *Am. J. Anat.* **165**, 373–384
46. Li, X., Zhang, Y., Kang, H., Liu, W., Liu, P., Zhang, J., Harris, S. E., and Wu, D. (2005) Sclerostin binds to LRP5/6 and antagonizes canonical Wnt signaling. *J. Biol. Chem.* **280**, 19883–19887
47. Klein-Nulend, J., Bakker, A. D., Bacabac, R. G., Vatsa, A., and Weinbaum, S. (2013) Mechanosensation and transduction in osteocytes. *Bone* **54**, 182–190
48. Boccafoschi, F., Mosca, C., Bosetti, M., and Cannas, M. (2011) The role of mechanical stretching in the activation and localization of adhesion proteins and related intracellular molecules. *J. Cell. Biochem.* **112**, 1403–1409
49. Baron, R., and Kneissel, M. (2013) WNT signaling in bone homeostasis and disease: from human mutations to treatments. *Nat. Med.* **19**, 179–192
50. Van Bezooijen, R. L., Svensson, J. P., Eefting, D., Visser, A., van der Horst, G., Karperien, M., Quax, P. H., Vrieling, H., Papapoulos, S. E., ten Dijke, P., and Löwik, C. W. (2007) Wnt but not BMP signaling is involved in the inhibitory action of sclerostin on BMP-stimulated bone formation. *J. Bone Miner. Res.* **22**, 19–28
51. Zhang, C., Cho, K., Huang, Y., Lyons, J. P., Zhou, X., Sinha, K., McCrea, P. D., and de Crombrugghe, B. (2008) Inhibition of Wnt signaling by the osteoblast-specific transcription factor osterix. *Proc. Natl. Acad. Sci. USA* **105**, 6936–6941
52. Yang, F., Tang, W., So, S., de Crombrugghe, B., and Zhang, C. (2010) Sclerostin is a direct target of osteoblast-specific transcription factor osterix. *Biochem. Biophys. Res. Commun.* **400**, 684–688
53. Nakashima, K., Zhou, X., Kunkel, G., Zhang, Z., Deng, J. M., Behringer, R. R., and de Crombrugghe, B. (2002) The novel zinc finger-containing transcription factor osterix is required for osteoblast differentiation and bone formation. *Cell* **108**, 17–29
54. Matsubara, T., Kida, K., Yamaguchi, A., Hata, K., Ichida, F., Meguro, H., Aburatani, H., Nishimura, R., and Yoneda, T. (2008) BMP2 regulates osterix through Msx2 and Runx2 during osteoblast differentiation. *J. Biol. Chem.* **283**, 29119–29125

Received for publication February 19, 2019.
Accepted for publication May 28, 2019.